AGU100 ADVANCING EARTH AND SPACE SCIENCE

Geophysical Research Letters

RESEARCH LETTER
10.1029/2018GL078185

Key Points:
- A new pixel-scale method is developed to compute backscattering of non-algal particles from ocean color data
- The backscattering of non-algal particles has geographical variability from northern to southern hemispheres
- The backscattering of non-algal particle variability has to be taken into account in phytoplankton biomass models

Supporting Information:
- Supporting Information S1

Correspondence to:
M. Bellacicco,
marco.bellacicco@obs-vlfr.fr

Citation:
Bellacicco, M., Volpe, G., Briggs, N., Brando, V., Pitarch, J., Landolfi, A., et al. (2018). Global distribution of non-algal particles from ocean color data and implications for phytoplankton biomass detection. *Geophysical Research Letters*, *45*, 7672–7682. https://doi.org/10.1029/2018GL078185

Received 17 APR 2018
Accepted 16 JUL 2018
Accepted article online 24 JUL 2018
Published online 11 AUG 2018

Global Distribution of Non-algal Particles From Ocean Color Data and Implications for Phytoplankton Biomass Detection

M. Bellacicco[1,2], G. Volpe[2], N. Briggs[1,3], V. Brando[2], J. Pitarch[4], A. Landolfi[5], S. Colella[2], S. Marullo[6], and R. Santoleri[2]

[1]Sorbonne Université, CNRS, Laboratoire d'Océanographie de Villefanche (LOV), Villefranche-sur-mer, France, [2]Institute of Atmospheric Sciences and Climate (ISAC)-CNR, Rome, Italy, [3]National Oceanographic Center, Southampton, UK, [4]Department of Coastal Systems, Royal Netherlands Institute for Sea Research, Texel, Netherlands, [5]Marine Biogeochemical Modelling, GEOMAR Helmholtz-Zentrum für Ozeanforschung Kiel, Kiel, Germany, [6]Italian National Agency for New Technologies, Energy and Sustainable Economic Development (ENEA), Frascati, Italy

Abstract In the last few decades, phytoplankton biomass has been commonly studied from space. However, satellite analysis of non-algal particles (NAPs), including heterotrophic bacteria and viruses, is relatively recent. In this work, we estimate the backscattering coefficient associated with the NAP fraction that does not covary with chlorophyll based on satellite particulate backscattering coefficient and chlorophyll (b_{bp}NAP). b_{bp}NAP is computed at 100-km resolution using 19 years of monthly satellite data. We find clear differences in b_{bp}NAP between northern and southern oceans. High b_{bp}NAP values are found in the Arctic and Southern Oceans, the North Atlantic area influenced by the Gulf Stream current, as well as shelf regions (i.e., Patagonian shelf) affected by upwelling regimes. Low correlation between chlorophyll and backscattering prevents precise b_{bp}NAP estimations in oligotrophic areas (e.g., subtropical gyres). These b_{bp}NAP estimations lead to a reduction to half in satellite-based phytoplankton biomass estimates respect to previously published results.

Plain Language Summary In the ocean, there are different seawater constituents that contribute to the inherent optical properties: Phytoplankton is a major constituent and one of the most studied in the last decade. Other important constituents are the colored dissolved organic matter and non-algal particles (NAPs). NAP includes (i) heterotrophic organisms such as bacteria, micrograzers, and viruses; (ii) detrital organic particles such as fecal pellets and cell debris; and (iii) mineral particles of both biogenic (e.g., calcite liths and shells) and terrestrial origin (e.g., clays and sand). This study is the first attempt to define the NAP from space, and its spatial variability, and how it contributes to refine the phytoplankton carbon biomass estimation. We estimate the backscattering coefficient associated with the NAP fraction that does not covary with chlorophyll from the satellite particulate backscattering coefficient and chlorophyll (bbpNAP). Our main results evidence a geographical variability of bbpNAP from northern to southern oceans with two distinct regimes: one associated with the productive areas in which bbpNAP and biomass are anticorrelated and another in which bbpNAP high values are in regions dominated by inorganic origin. We demonstrate that the spatial variability of bbpNAP should not be ignored.

1. Introduction

In the ocean, there are different seawater constituents that contribute to the inherent optical properties. Phytoplankton is a major constituent and one of the most studied in the last decade (e.g., its space-temporal variability, physiology, and ecology; Siegel et al., 2013; Halsey & Jones, 2015). Other important constituents are colored dissolved organic matter (CDOM) and non-algal particles (NAPs). NAP includes (i) heterotrophic organisms such as bacteria, micrograzers, and viruses; (ii) detrital organic particles such as fecal pellets and cell debris; and (iii) mineral particles of both biogenic (e.g., calcite liths and shells) and terrestrial origin (e.g., clays and sand; Sosik, 2008, and references therein). While phytoplankton and CDOM are quite well studied at global scale, the optical properties of these particles are not well known. In particular, the total NAP absorption spectrum tends to monotonically increase with decreasing wavelengths, similar to that observed for CDOM (e.g., Iturriaga & Siegel, 1989; Nelson et al., 1998; Roesler et al., 1989; Sosik & Mitchell, 1995). Several studies have investigated the absorption of NAP (Bricaud et al., 2010; Sosik, 2008, and reference therein), but

patterns of NAP backscattering in the surface ocean are not fully studied (Cho & Azam, 1990; Stramski & Kiefer, 1991) because direct measurements of fractionated b_{bp} in the field are not possible using current technology. However, we can gain some insight into the constituents of particulate backscattering b_{bp} by separating the fraction that covaries with phytoplankton from the fraction that does not covary.

In this context, a first attempt to define the backscattering due to NAP from space was suggested by Behrenfeld et al. (2005), who proposed an equation for phytoplankton carbon biomass estimation from satellite, based on a linear relationship between particulate backscattering coefficient (b_{bp}) and chlorophyll (Chl). In their model, the b_{bp}NAP coefficient, which is defined as the fraction of backscattering due to non-algal particles (e.g., stable heterotrophic and detrital components of the surface particle population in open ocean) that does not covary with Chl, is assumed constant in space and time (Behrenfeld et al., 2005; for more details on the b_{bp}NAP computation see paragraph 2.2.). Behrenfeld's method has been applied in many recent works: Westberry et al. (2008), Siegel et al. (2013), Mignot et al. (2014), Behrenfeld et al. (2016), Westberry et al. (2016), Thomalla et al. (2017), among others.

This method has been used to estimate phytoplankton carbon biomass in terms of mg C m^{-3} and the Chl:C ratio in photoacclimation studies (Behrenfeld et al., 2016; Bellacicco et al., 2016; Halsey & Jones, 2015; MacIntyre et al., 2002) and applied in phytoplankton physiology studies from space as well as biogeochemical models (Arteaga et al., 2014; Bellacicco et al., 2016; Halsey & Jones, 2015; Siegel et al., 2013).

Recently, Bellacicco et al. (2016) computed b_{bp}NAP in a 3-month window in predefined bioregions of the Mediterranean Sea (Lavigne et al., 2013) and found both marked seasonal and regional b_{bp}NAP variabilities. Their results supported in situ observations in the Mediterranean Sea (Siokou-Frangou et al., 2010), suggesting that the heterotrophic and detrital components of the surface particle pool are neither negligible (Morel, 1988) nor stable, but highly dynamic in both space and time. In Bellacicco et al. (2016) the Chl-b_{bp} relationship was found to be highly dependent on the season and on the biogeochemistry of the area, similarly as in Antoine et al. (2011, their Figure 10). These findings suggest that the use of the global b_{bp}NAP constant coefficient (Behrenfeld et al., 2005) can result in an overestimation of phytoplankton biomass, in the Mediterranean Sea.

High covariability between Chl and b_{bp} is expected because phytoplankton cells contain Chl and also act as light scatterers. In addition, the unpigmented NAP also contributes to the b_{bp} signal and is known to exhibit patterns of variability similar to that of phytoplankton biomass (Bellacicco et al., 2016). The degree of covariability between Chl and b_{bp} provides a means for assessing the role that the physiological state of phytoplankton cells plays in modulating the biomass concentration and how it is perceived from remote sensing observations (Bellacicco et al., 2016, and references therein). High Chl-b_{bp} covariability is a clear indication that particles (and biomass) covary also with phytoplankton abundance, with the physiological photoacclimation process playing a negligible role in the Chl detection from space. On the other hand, when the range of variability of b_{bp} is narrower than that of Chl, covariability is low and Chl detected from space is dominated by the photoacclimation process (Barbieux et al., 2018; Behrenfeld et al., 2005; Bellacicco et al., 2016; Halsey & Jones, 2015).

There can be a number of reasons for which the Chl-b_{bp} relationship will vary both in space and time. These include the ratio of NAP to phytoplankton biomass, variability in phytoplankton carbon-to-Chl ratio (Bellacicco et al., 2016), and the species composition and diversity (e.g., size and shape) of phytoplankton cells and nature of the NAP itself (Dall'Olmo et al., 2009, 2012; Stramski et al., 2004).

When this intrinsic variability dominates over the variability in biomass, null or negative correlations can be obtained violating the assumptions for the calculation of b_{bp}NAP (i.e., in the ultraoligotrophic oceanic areas).

Filling the knowledge gap about the global scale b_{bp}NAP variability can surely improve our understanding of its main components and enhancing the estimation of the phytoplankton carbon from space. Heterotrophic bacteria, part of b_{bp}NAP, are the crucial connection among detritus, dissolved organic matter, and higher trophic levels (Bellacicco et al., 2016; Siokou-Frangou et al., 2010). Similarly, the ecological role of calcifying phytoplankton has been widely documented in certain oceanic regions (e.g., Southern Ocean; Balch, 2018; Balch et al., 2016, and references therein) where the impact of their calcium carbonate coccoliths, also part of b_{bp}NAP, may be assessed via space-born observations of the backscattering coefficient (Balch et al., 1999). Open research questions on b_{bp}NAP estimates from space are as follows:

i Does b_{bp}NAP vary in space on a global scale?
ii Does b_{bp}NAP spatial variability impact phytoplankton carbon biomass estimation?

In this paper, we aim to answer these questions by extending the Behrenfeld et al. (2005) and Bellacicco et al. (2016) methodologies to develop a global map of mean b_{bp}NAP along with a first evaluation of its potential impact on phytoplankton carbon biomass estimation.

2. Data and Methods

2.1. Satellite Data

The full European Space Agency (ESA) Ocean Color-Climate Change Initiative version 3 monthly Chl (mg m^{-3}) and b_{bp} (m^{-1}; 443 nm) data time series at 4-km resolution for the period 1997–2015 over the global ocean was downloaded from the ESA-CCI website (http://www.esa-oceancolour-cci.org/). ESA-CCI products are the results of the merging between Sea-Viewing Wide Field-of-View Sensor, Medium-Resolution Imaging Spectrometer, Moderate Resolution Imaging Spectroradiometer-Aqua, and Visible Infrared Imaging Radiometer Suite time series (Brewin et al., 2015; Mélin & Sclep, 2015; Mélin et al., 2017; Sathyendranath et al., 2017). Chl was estimated with a blending of the OCI (as implemented by NASA, itself a combination of CI and OC4), the OC5 (NASA, 2010), and the OC3 algorithms (http://www.esa-oceancolour-cci.org/?q=webfm_send/684). The Quasi Analytical Algorithm was used to compute b_{bp} (Lee, 2014; Lee et al., 2002). The accuracy of the Quasi Analytical Algorithm was demonstrated in Brewin et al. (2015), and also by Pitarch et al. (2016) and Bellacicco et al. (2016), and previous works of Mélin et al. (2005, 2011). A thorough analysis on the uncertainties of both parameters is available on the ESA OC-CCI website or on the Product User Guide. Both data sets were remapped at 100-km resolution, enough to resolve the broader oceanographic scales of variability.

2.2. b_{bp}NAP Computation

The b_{bp}NAP model is based upon the approach of Behrenfeld et al. (2005), who estimated global b_{bp}NAP as the intercept of the least square linear regression fit between Chl and b_{bp}; that is, b_{bp}NAP is b_{bp} when Chl is zero. They estimated a unique constant value (0.00035 m^{-1}; their Figure 1) using the entire multiyear global data set.

In this work, the technique developed by Bellacicco et al. (2016) is extended to compute b_{bp}NAP at the scale of the satellite pixel, rather than using predefined bioregions, allowing the analysis of its spatial variability along the entire global ocean. The proposed equation for b_{bp}NAP is

$$b_{bp}\mathrm{NAP} = b_{bp} - k\ \mathrm{Chl} \tag{1}$$

with k being the slope of the least square regression fit between Chl and b_{bp} single-pixel time series. b_{bp}, Chl, and hence b_{bp}NAP are resolved at pixel scale. The term kChl is the fraction of b_{bp} that covaries with Chl. The b_{bp}NAP was computed using a broader 3 × 3 pixel spatial window to increase statistical robustness of the regression fit. A quality control was applied to the data before computing the fit, and the outliers were discarded using three standard deviation confidence limit.

The b_{bp}NAP pixel-based estimations (Figure S1 in the supporting information), obtained from a regression between Chl and b_{bp} on a pixel scale with a statistical significance (S) less than 0.95 (computed through the Student t test), were not considered in the analysis and were masked out. In addition, pixels in which the Pearson correlation coefficient, r, was lower than 0 were not considered in the computation of b_{bp}NAP and b_{bp}NAP:b_{bp} ratio (hereafter b_{bp}NAP~). σbbpNAP is estimated as the standard deviation of the intercept for each regression. The coefficient of variation is then CV = σbbpNAP/bbpNAP at pixel scale to show the relative uncertainty of the b_{bp}NAP estimates. Figure S2 shows the robustness of b_{bp}NAP estimate at 99% confidence level.

The b_{bp}NAP pixel-based estimates are then used to compute phytoplankton carbon biomass (mg C m^{-3}; Figure 3a) following Behrenfeld et al. (2005, see their paragraph 3.1) and Bellacicco et al. (2016, see their equation (1)), but using the b_{bp}NAP spatially resolved (Figure 2a) instead of a single constant value (0.00035 m^{-1}):

$$\mathrm{Carbon} = \left[b_{bp} - b_{bp}\mathrm{NAP}\right] * \mathrm{SF} \tag{2}$$

where SF is the scaling factor chosen for satellite Chl:C ratio values to be consistent with laboratory results, and for the average contribution of phytoplankton to total particulate organic carbon to be consistent with field estimate: It is equal to 13,000 mg C m^{-2} (Behrenfeld et al., 2005).

Finally, we calculate the relative percentage difference (RPD) between phytoplankton carbon computed with single b_{bp}NAP coefficient (Behrenfeld et al., 2005) and the carbon as computed in equation (2):

$$\mathrm{RPD} = 100 * \frac{\left[\mathrm{Carbonsingle}_{\mathrm{bbpNAP}} - \mathrm{Carbon}\right]}{\mathrm{Carbon}} \tag{3}$$

2.3. The Chl-b_{bp} Relationship for b_{bp}NAP Estimation

Here to guide the interpretation of the b_{bp}NAP distribution, the biogeochemical implications of the Chl-b_{bp} relationship (equations (1) and (2)) are presented. Figures 1a and 1b show the climatological maps of b_{bp} and Chl, respectively. The b_{bp} and Chl patterns of variability are coherent in the productive areas like the polar regions, the coastal upwelling, and along the equatorial belts of the Atlantic and Pacific oceans. There are areas in which the Chl and b_{bp} maps show differences: In the equatorial Atlantic between 10°S and 10°N, Chl shows high values, but b_{bp} does not. North and south of this belt, the Chl map clearly displays the presence of the subtropical gyres, while the b_{bp} map presents a uniform area of low values which extends from the equator to 30°N/S. The oligotrophic pattern of the South Pacific Subtropical Gyre shows different spatial extent when observed through Chl and b_{bp}. Figure 1b shows that South Pacific Subtropical Gyre extends more to the south toward the Antarctic Circumpolar Current than shown by Figure 1a. Similarly, in the Pacific Equatorial upwelling system, high Chl extends more to the west than b_{bp}, resulting in the latitudinal thickness of the Chl pattern to be more pronounced than b_{bp}. Globally, Chl and b_{bp} vary over more than 3 orders of magnitude, also showing similar geographical patterns (Figures 1a and 1b).

Figure 1c shows the Pearson coefficient (*r*) between Chl and b_{bp} time series obtained using 19 years of satellite data. Two main considerations emerge: Nearly the entire global ocean presents significant positive correlation, and in most areas, this correlation is high, meaning that either b_{bp} or Chl can be used for determining the phytoplankton dynamics and distribution, as expected in case I waters. This type of relationship is the underpinning basis for the estimation of b_{bp}NAP. However, this Chl-b_{bp} relationship falls short in the subtropical gyres, where *r* shows null or negative values. Two main reasons can contribute to this poor relationship: First, the photoacclimation process, known to be dominant in such areas (e.g., Barbieux et al., 2018; Siegel et al., 2013), introduces variability in Chl that is uncoupled with biomass, and second, ocean color can only sample the few upper meters of the water column, under the deep chlorophyll maximum conditions (Volpe et al., 2012), and thus, the phytoplankton vertical distribution is such that most of the algal biomass is out of the satellite detection. This in part explains the extremely oligotrophic character that these areas display when sampled through ocean color remote sensing (Volpe et al., 2007).

3. Results and Discussion

3.1. The Spatial Distribution of b_{bp}NAP and CV

The pattern of b_{bp}NAP (Figure 2a) generally disagrees with the Chl geographical distribution, with lowest values in the most productive regions. For example, in the eastern portion of the productive subpolar North Atlantic, b_{bp}NAP is low relative to the area just south influenced by the Gulf Stream current. High b_{bp}NAP values are found in several hotspots around the globe, many with moderate or variable Chl, such as the north border of the North Atlantic subtropical gyre, in several bands across the Southern Ocean, the southeast coast of Australia, and the southwest tip of South America. Other b_{bp}NAP hotspots, however, do coincide with high Chl, including the eastern continental shelf of North America, the northern Benguela upwelling region, and the Barents and North Seas.

The median b_{bp}NAP value computed using all the valid pixels of the global ocean is 9.5 10^{-4} m^{-1}, very close to the median value found for the Mediterranean Sea (0.001 m^{-1}; Bellacicco et al., 2016). The coefficient of 3.5 10^{-4} m^{-1} found by Behrenfeld et al. (2005) for b_{bp}NAP is much lower than this value and falls in the second percentile of the b_{bp}NAP frequency distribution (see histogram on Figure 2a; vertical white line). Despite the various possible sources of discrepancy between the two methods (ocean color algorithms and processing, length of data time series, and averaging aggregation methods), the distribution of the 99% b_{bp}NAP confidence interval (Figure S2) evidences that most of the b_{bp}NAP values computed here vary only ~5%. The b_{bp}NAP found here spans over more than 1 order of magnitude and is in line with the range of

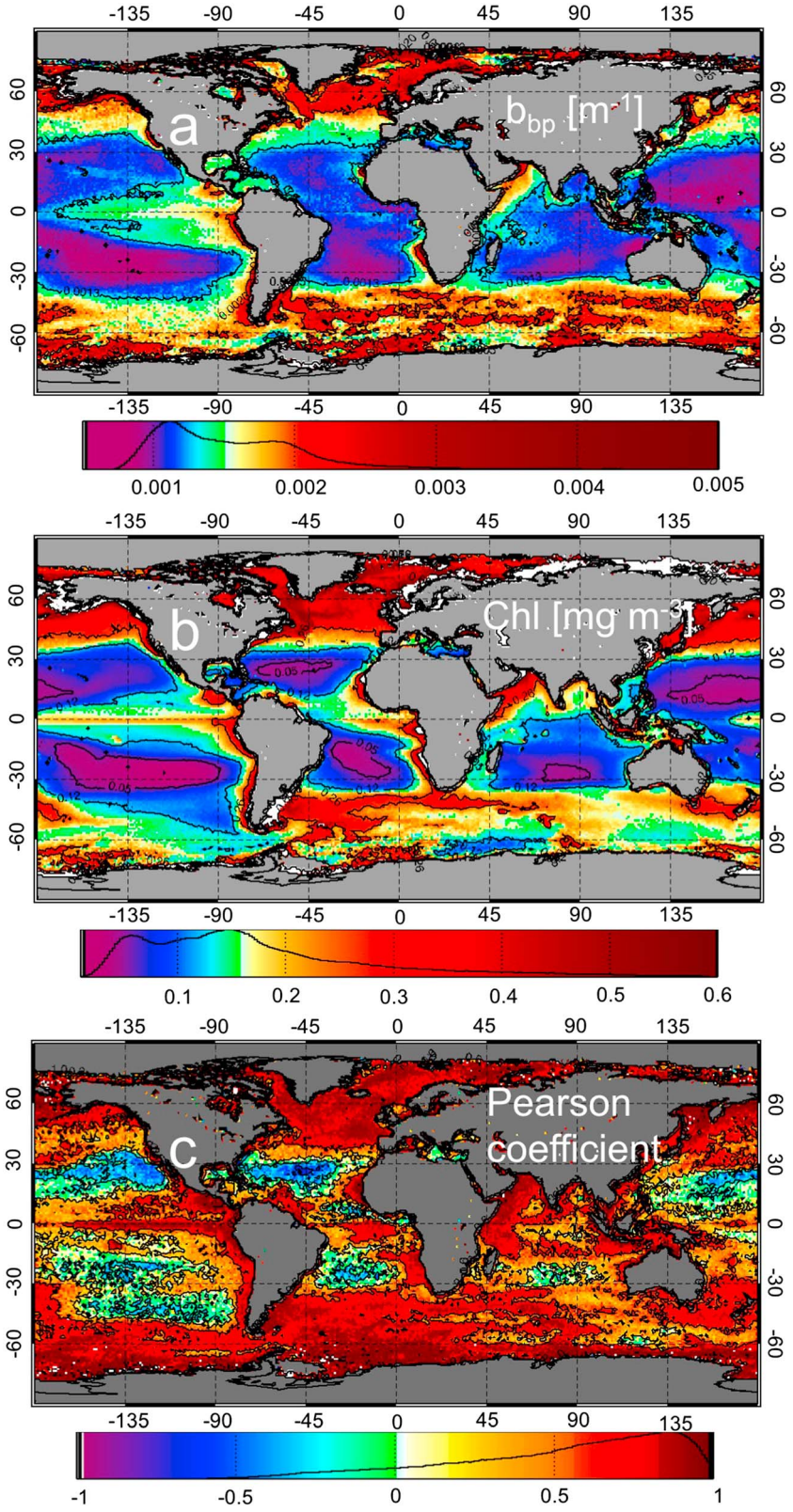

Figure 1. Annual climatology of (a) b_{bp}, (b) Chl, and (c) Pearson coefficient between Chl and b_{bp}. In case of the subtropical gyres, the Pearson coefficient is ≤ 0, while in case of other areas of the global ocean, the coefficient is always >0 and close to 1. The frequency distribution histogram is overlaid in the three color bars.

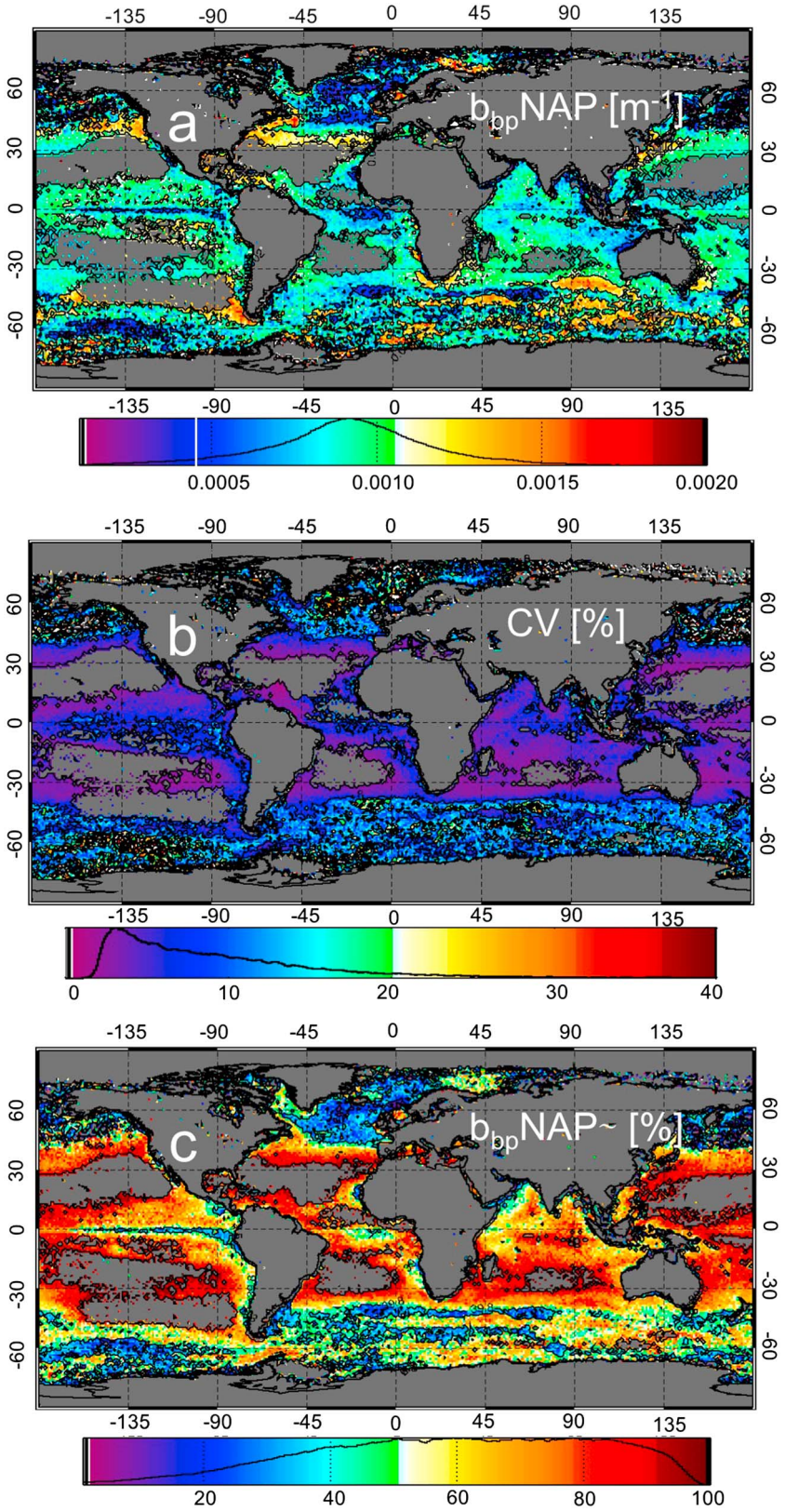

Figure 2. Maps of (a) b_{bp}NAP, (b) CV, and (c) b_{bp}NAP~. The frequency distribution histogram is overlaid in the three color bars in order to show the recurrence of high values of each parameter. Pixels in which the Pearson coefficient (*r*) was ≤0 and statistical significance (*S*) was less than 0.95 were not considered in the analysis (gray areas).

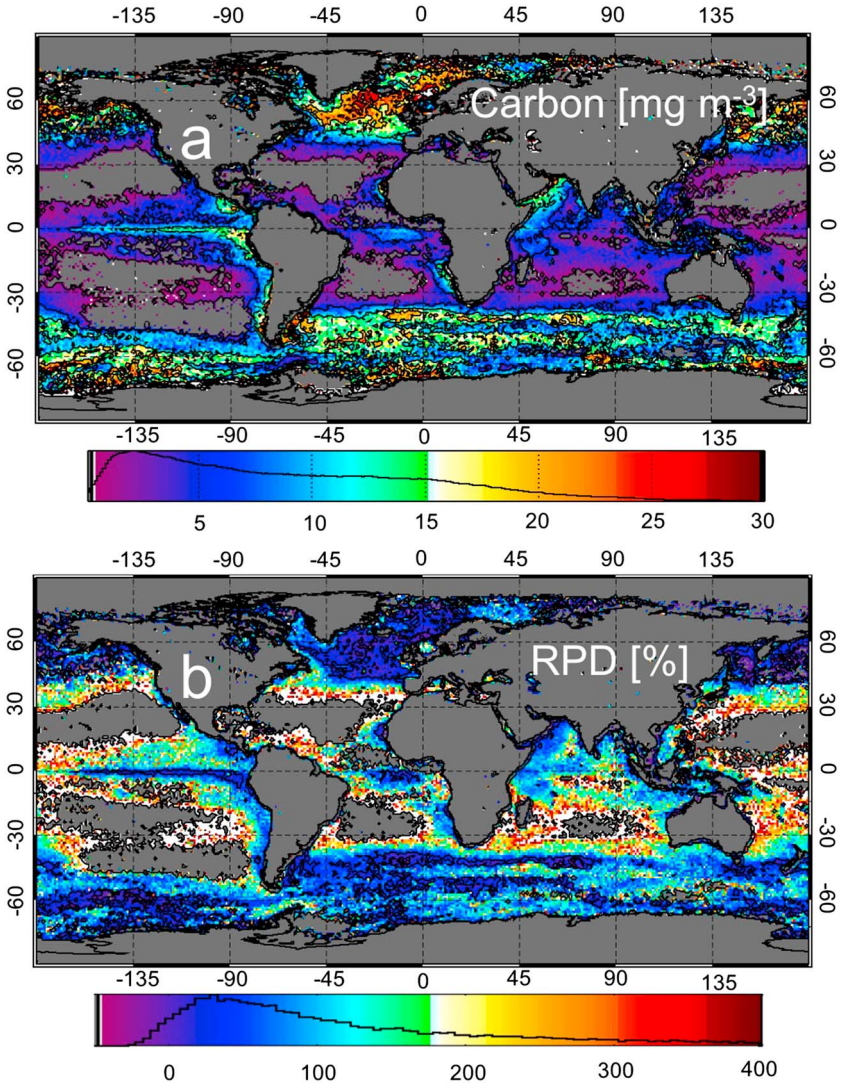

Figure 3. (a) Map of phytoplankton carbon biomass computed using the b_{bp}NAP spatially resolved at pixel scale; RPD map between phytoplankton carbon biomass using the b_{bp}NAP, as computed in this work, and a single b_{bp}NAP coefficient. Pixels in which the Pearson coefficient (*r*) was ≤0 and statistical significance (*S*) was less than 0.95 were not considered in the analysis (gray areas). The frequency distribution histogram is overlaid in the two color bars in order to show the recurrence of high values of parameters. Note that RPD over 150 occurred at the boarder of the gyres and thus has to be interpreted with caution (see also the paragraph on spatial distribution of b_{bp}NAP~).

variability found by Brewin et al. (2012, their Table 3] from NOMAD, equatorial Pacific, and North Atlantic data set (3.6–7.2 10^{-4} m^{-1}) and Graff et al. (2015, their Table 2 and Figure 3) from a data set in the equatorial Pacific and AMT cruises (3.9–10.8 10^{-4} m^{-1}), but readers must be aware of the different temporal and spatial scales used to derive the former b_{bp}NAP estimates.

b_{bp}NAP CV presents low values at low midlatitudes and higher values at high latitudes (Figure 2b). CV rarely exceeds 25% with the most frequent value below 5% in correspondence of the margins of the main ocean gyres. These areas are characterized both by high b_{bp}NAP and lower covariability in the Chl-b_{bp} relationship. On the other hand, CV is higher at the high latitudes, which is due partly to higher variability in the Chl-b_{bp} relationship (southern hemisphere) and partly to very low b_{bp}NAP (esp. in the North Atlantic). Figure S1 is a graphical representation of the method for the b_{bp}NAP determination, which is supported by statistical analysis of the Chl-b_{bp} relationship.

One could argue that the b_{bp}NAP computation and assessment should be limited to the midrange of Chl values, avoiding the clear-water conditions (already limited by our criteria), and very high Chl values typical of the coastal waters. In this latter case, the relationship between Chl and b_{bp} tends again to flatten out, and consequently, the correlation is expected to be low, so our flagging criteria based on correlation value avoid b_{bp}NAP computation in coastal areas. In any case, the coastal pixels do not significantly contribute to the distribution, since our spatial resolution is low (100 km). This is also confirmed by the frequency distribution of b_{bp}NAP (see Figure 2a). The pixels referred to open ocean represented the main domain (>70%).

3.2. The Spatial Distribution of b_{bp}NAP~

b_{bp}NAP~(Figure 2c; here defined as the fraction of b_{bp}NAP with respect to the total b_{bp}; in percentage) follows the inverse of the biomass spatial variability as a consequence of the higher relative variability in b_{bp} versus b_{bp}NAP. Indeed, in the North Atlantic Ocean, characterized by high biomass, b_{bp}NAP is lower than 30% of total b_{bp}, while it reaches values over 60% in the area influenced by the Gulf Stream current (at the border of the North Atlantic subtropical gyre). This pattern is consistent with expectations if b_{bp} is dominated by organic matter: In oligotrophic regions, perennial nutrient limitation drives low phytoplankton biomass, which is rapidly recycled in the surface layer, in turn supporting relatively high bacterial, small heterotrophic, and detrital biomass (Barbieux et al., 2018, and references therein). Similarly, in the productive North Atlantic, b_{bp}NAP~ is consistently low with the high biomass values observed during the spring bloom (Alkire et al., 2014, and references therein).

At the borders of the gyres, b_{bp}NAP exceeds 80% of the total b_{bp}. Here however, Chl-b_{bp} correlation values are lower than 0.5, suggesting that the theoretical thresholds that we applied ($r > 0$, $S > 95\%$) should be more stringent in excluding or including pixels from the analysis. High b_{bp}NAP~ could be due to high year-round NAP. Low b_{bp}NAP~ could be either due to low NAP or because NAPs are strongly correlated with Chl.

In the North Atlantic Ocean, b_{bp} appears to be dominated more by particles that covary with phytoplankton cells, as opposed to the Southern Ocean, in which b_{bp} seems to be dominated more by particles that do not covary with total phytoplankton biomass. Indeed, b_{bp}NAP ~shows hot spots in the Southern Ocean with values >70% (e.g., Patagonia shelf and along the Antarctic Circumpolar Current). In that respect, the b_{bp}NAP measurements, and its order of magnitude, are consistent with the results found by Balch et al. (2016, their Figure 2: b_b' transect of in situ data) along the entire Southern Ocean. Balch et al. (2016) found that the b_{bp} associated with particulate inorganic carbon (e.g., coccoliths) ranges between 0 and 1.0 10^{-3} m^{-1}. Here b_{bp}NAP in the same area ranges between 5 10^{-4} and 1.5 10^{-3} m^{-1}, and b_{bp}NAP~ is around 80%. This suggests coccoliths being the driving signal of b_{bp}NAP in the Southern Ocean. Indeed, coccoliths covary with b_{bp} because they scatter light as all other particles have a b_{bp} signal. Thus, the b_{bp}NAP is reasonably related to the coccolithophorid seasonality (i.e., skeleton compounds of no longer living cells; b_{bp}NAP is the b_{bp} when Chl is zero). On the other hand, in the North Atlantic Ocean, where b_{bp}NAP~ is less than 30%, b_{bp} is dominated by the particles that covary with phytoplankton cells (see equation (1)), thus being more determined by phytoplankton dynamics.

3.3. Implications for Phytoplankton Carbon Biomass From Satellite

Our analysis shows that b_{bp}NAP accounts for between 20 and 80% of the b_{bp} signal (e.g., from North Atlantic to Southern Oceans). Thus, we recommend taking into account the variability of this term when estimating phytoplankton carbon from b_{bp}. To estimate the impact of varying b_{bp}NAP on the satellite-derived carbon estimation, we computed the global map of phytoplankton carbon using the b_{bp}NAP estimated here (Figures 2a and 3a). The spatial pattern of phytoplankton carbon (Figure 3a) generally agrees with the Chl geographical distribution (Figure 1b) with high values in the most productive regions such as the polar regions, the coastal upwelling, and along the equatorial belts of the Atlantic and Pacific oceans. Low values are located in correspondence of midlatitude areas such as the boundaries of the gyres (Figure 3a). However, variable b_{bp}NAP estimates have a strong impact on quantitative phytoplankton biomass estimates, yielding a median value of 8.6 mg C m^{-3} when considering all the pixels (both open and coastal waters) and 8.07 mg C m^{-3} considering only pixels in open ocean. When single value estimated by Behrenfeld et al. (2005) is used instead, we obtain much higher median estimates of 16.6 and 16.19 mg C m^{-3}, respectively (Figure 3a). The use of spatially varying b_{bp}NAP instead of the single coefficient dramatically impacts the

phytoplankton carbon estimates from space. Indeed, in the North Atlantic Ocean, b_{bp}NAP does not significantly deviate from the constant coefficient found by Behrenfeld et al. (2005, Figure 3b; RPD lower than 10%). On the other hand, in regions dominated by b_{bp}NAP of inorganic nature not covarying with Chl, such as the Southern Ocean, the computation of phytoplankton carbon via b_{bp} exhibits large differences: RPD values greater than 100% (Figure 3b). The order of magnitude of our phytoplankton carbon biomass is consistent with the recent estimates of phytoplankton carbon by Arteaga et al. (2016) computed with a biogeochemical model able to resolve the Chl:C ratio and accounting for the optical acclimation of phytoplankton to nutrient, light, and temperature. A future challenge concerns to take into account the change of the scaling factor relating b_{bp} to C, as reported in Kostadinov et al. (2009, 2010, 2016), coupled with the b_{bp}NAP spatial variability as found in this work. Kostadinov et al. (2016) developed a carbon-based phytoplankton size class approach from satellite data considering the variation of the particle size distribution that influences the scaling factor. In this way, the phytoplankton carbon from space should consider both the changes in the particle size distribution that impact on backscattering per unit C biomass due to different scattering efficiencies and the b_{bp}NAP coefficient. It should increase the efficiency of phytoplankton carbon biomass retrieval from ocean color remote sensing data. To date, the impact of the Chl:C ratio, and thus of the SF term, on phytoplankton carbon computation is still not known. Future studies should be aimed at evaluating whether the variability induced by the SF term piles up or reduces the one induced by b_{bp}NAP in the computation of phytoplankton carbon biomass (Arteaga et al., 2016).

4. Conclusions

Pixel-scale estimations showed marked b_{bp}NAP geographical variability. In productive regions, such as the North Atlantic Ocean, b_{bp}NAP and biomass are anticorrelated. This is presumably because nearly all NAP is strongly correlated with Chl, while in less productive regions with shallower winter mixed layers, there is a more constant population of noncovarying bacteria and detritus. In regions containing NAP of inorganic origin, including some coastal regions and the calcite belt of the Southern Ocean, we find high b_{bp}NAP values. Within the subtropical gyres, b_{bp}NAP could not be estimated, due to lack of positive correlation between satellite b_{bp} and Chl estimates, likely driven by photoacclimation. Throughout most of the ocean, our spatially resolved b_{bp}NAP estimates were higher than the single estimate calculated by Behrenfeld et al. (2005). These higher b_{bp}NAP estimates had a large impact on estimates of phytoplankton biomass from satellite b_{bp}. Our median phytoplankton C estimate in the pixels considered (8.6 mg C m^{-3}) was roughly half of the median estimate obtained using a single b_{bp}NAP estimate (16.6 mg C m^{-3}). Although we currently lack sufficient in situ phytoplankton carbon estimates to validate either estimate at global scale, our results strongly suggest that spatial variability in b_{bp}NAP should not be ignored.

Future work in this research pathway should (1) focus on comparing existing in situ inherent optical property data (i.e., BGC-Argo) to satellite products without leaving out the collection of in situ optical and plankton carbon data, (2) validate the impact of b_{bp}NAP variability on phytoplankton carbon estimation from space, and (3) give insight on the actual composition of b_{bp}NAP in various zones of the world ocean. Finally, inclusion of the reported relationships into phytoplankton carbon models will help improve their predictions.

Acknowledgments
M.B. started this work funded by the fellowship RITMARE at the Institute of Atmospheric Sciences and Climate (ISAC) of the Italian Research National Council (CNR). Now M.B. is at the Laboratoire d'Océanographie de Villefranche sur Mer (LOV) with a postdoctoral fellowship funded by the Centre Nationales d'Etudes Spatiales (CNES, Paris, France). N.B. collaborated at LOV, and now N.B. is on the National Oceanographic Center (NOC) of Southampton (UK). A special thanks to the ESA Ocean Color-Climate Change Initiative team for providing free access to the data time series (http://www.esa-oceancolour-cci.org). Special thanks to Francesco Bignami and Sorin Constantin for their criticism and suggestions.

References

Alkire, M. B., Lee, C., D'Asaro, E., Perry, M. J., Briggs, N., Cetinić, I., & Gray, A. (2014). Net community production and export from Seaglider measurements in the North Atlantic after the spring bloom. *Journal of Geophysical Research: Oceans*, *119*, 6121–6139. https://doi.org/10.1002/2014JC010105

Antoine, D., Siegel, D. A., Kostadinov, T., Maritorena, S., Nelson, N. B., Gentili, B., et al. (2011). Variability in optical particle backscattering in contrasting biooptical oceanic regimes. *Limnology and Oceanography*, *56*(3), 955–973. https://doi.org/10.4319/lo.2011.56.3.0955

Arteaga, L., Pahlow, M., & Oschlies, A. (2014). Global patterns of phytoplankton nutrient and light colimitation inferred from an optimality-based model. *Global Biogeochemical Cycles*, *28*, 648–661. https://doi.org/10.1002/2013GB004668

Arteaga, L., Pahlow, M., & Oschlies, A. (2016). Modeled Chl: C ratio and derived estimates of phytoplankton carbon biomass and its contribution to total particulate organic carbon in the global surface ocean. *Global Biogeochemical Cycles*, *30*, 1791–1810. https://doi.org/10.1002/2016GB005458

Balch, W. M. (2018). The ecology, biogeochemistry, and optical properties of coccolithophores. *Annual Review of Marine Science*, *10*(1), 71–98. https://doi.org/10.1146/annurev-marine-121916-063319

Balch, W. M., Bates, N. R., Lam, P. J., Twining, B. S., Rosengard, S. Z., Bowler, B. C., et al. (2016). Factors regulating the Great Calcite Belt in the Southern Ocean and its biogeochemical significance. *Global Biogeochemical Cycles*, *30*, 1124–1144. https://doi.org/10.1002/2016GB005414

Balch, W. M., Drapeau, D. T., Cucci, T. L., Vaillancourt, R. D., Kilpatrick, K. A., & Fritz, J. J. (1999). Optical backscattering by calcifying algae: Separating the contribution of particulate inorganic and organic carbon fractions. *Journal of Geophysical Research*, *104*(C1), 1541–1558. https://doi.org/10.1029/1998JC900035

Barbieux, M., Uitz, J., Bricaud, A., Organelli, E., Poteau, A., Schmechtig, C., et al. (2018). Assessing the variability in the relationship between the particulate backscattering coefficient and the chlorophyll a concentration from a global biogeochemical-Argo database. *Journal of Geophysical Research*, *123*(2), 1229–1250. https://doi.org/10.1002/2017JC013030

Behrenfeld, M. J., Boss, E., Siegel, D. A., & Shea, D. M. (2005). Carbon-based ocean productivity and phytoplankton physiology from space. *Global Biogeochemical Cycles*, *19*, GB1006. https://doi.org/10.1029/2004GB002299

Behrenfeld, M. J., O'Malley, R. T., Boss, E. S., Westberry, T. K., Graff, J. R., Halsey, K. H., et al. (2016). Revaluating ocean warming impacts on global phytoplankton. *Nature Climate Change*, *6*(3), 323.

Bellacicco, M., Volpe, G., Colella, S., Pitarch, J., & Santoleri, R. (2016). Influence of photoacclimation on the phytoplankton seasonal cycle in the Mediterranean Sea as seen by satellite. *Remote Sensing of Environment*, *184*, 595–604. https://doi.org/10.1016/j.rse.2016.08.004

Brewin, R. J., Dall'Olmo, G., Sathyendranath, S., & Hardman-Mountford, N. J. (2012). Particle backscattering as a function of chlorophyll and phytoplankton size structure in the open-ocean. *Optics Express*, *20*(16), 17632–17652. https://doi.org/10.1364/OE.20.017632

Brewin, R. J., Sathyendranath, S., Müller, D., Brockmann, C., Deschamps, P. Y., Devred, E., et al. (2015). The ocean colour climate change initiative: III. A round-robin comparison on in-water bio-optical algorithms. *Remote Sensing of Environment*, *162*, 271–294.

Bricaud, A., Babin, M., Claustre, H., Ras, J., & Tièche, F. (2010). Light absorption properties and absorption budget of Southeast Pacific waters. *Journal of Geophysical Research*, *115*, C08009. https://doi.org/10.1029/2009JC005517

Cho, B. C., & Azam, F. (1990). Biogeochemical significance of bacterial biomass in the ocean's euphotic zone. *Marine Ecology Progress Series*, *63*, 253–259. https://doi.org/10.3354/meps063253

Dall'Olmo, G., Boss, E., Behrenfeld, M. J., & Westberry, T. K. (2012). Particulate optical scattering coefficients along an Atlantic meridional transect. *Optics Express*, *20*(19), 21532–21551. https://doi.org/10.1364/OE.20.021532

Dall'Olmo, G., Westberry, T. K., Behrenfeld, M. J., Boss, E., & Slade, W. H. (2009). Significant contribution of large particles to optical backscattering in the open ocean. *Biogeosciences*, *6*(6), 947–967. https://doi.org/10.5194/bg-6-947-2009

Graff, J. R., Westberry, T. K., Milligan, A. J., Brown, M. B., Dall'Olmo, G., van Dongen-Vogels, V., et al. (2015). Analytical phytoplankton carbon measurements spanning diverse ecosystems. *Deep Sea Research Part I: Oceanographic Research Papers*, *102*, 16–25.

Halsey, K. H., & Jones, B. M. (2015). Phytoplankton strategies for photosynthetic energy allocation. *Annual Review of Marine Science*, *7*(1), 265–297. https://doi.org/10.1146/annurev-marine-010814-015813

Iturriaga, R., & Siegel, D. A. (1989). Microphotometric characterization of phytoplankton and detrital absorption properties in the Sargasso Sea. *Limnology and Oceanography*, *34*(8), 1706–1726. https://doi.org/10.4319/lo.1989.34.8.1706

Kostadinov, T. S., Milutinović, S., Marinov, I., & Cabré, A. (2016). Carbon-based phytoplankton size classes retrieved via ocean color estimates of the particle size distribution. *Ocean Science*, *12*(2), 561–575.

Kostadinov, T. S., Siegel, D. A., & Maritorena, S. (2009). Retrieval of the particle size distribution from satellite ocean color observations. *Journal of Geophysical Research*, *114*, C09015. https://doi.org/10.1029/2009JC005303

Kostadinov, T. S., Siegel, D. A., & Maritorena, S. (2010). Global variability of phytoplankton functional types from space: Assessment via the particle size distribution. *Biogeosciences*, *7*(10), 3239–3257. https://doi.org/10.5194/bg-7-3239-2010

Lavigne, H., D'Ortenzio, F., Migon, C., Claustre, H., Testor, P., d'Alcalà, M. R., et al. (2013). Enhancing the comprehension of mixed layer depth control on the Mediterranean phytoplankton phenology. *Journal of Geophysical Research: Oceans*, *118*, 3416–3430. https://doi.org/10.1002/jgrc.20251

Lee, Z. (2014). Update of the Quasi-Analytical Algorithm (QAA_v6). http://www.ioccg.org/groups/Software_OCA/QAA_v6_2014209.pdf

Lee, Z., Carder, K. L., & Arnone, R.a. (2002). Deriving inherent optical properties from water color: A multiband quasi-analytical algorithm for optically deep waters. *Applied Optics*, *41*(27), 5755–5772. https://doi.org/10.1364/AO.41.005755

MacIntyre, H. L., Kana, T. M., Anning, T., & Geider, R. J. (2002). Photoacclimation of photosynthesis irradiance response curves and photosynthetic pigments in microalgae and cyanobacteria. *Journal of Phycology*, *38*(1), 17–38. https://doi.org/10.1046/j.1529-8817.2002.00094.x

Mélin, F., Berthon, J. F., & Zibordi, G. (2005). Assessment of apparent and inherent optical properties derived from SeaWiFS with field data. *Remote Sensing of Environment*, *97*(4), 540–553. https://doi.org/10.1016/j.rse.2005.06.002

Mélin, F., & Sclep, G. (2015). Band shifting for ocean color multi-spectral reflectance data. *Optics Express*, *23*(3), 2262–2279. https://doi.org/10.1364/OE.23.002262

Mélin, F., Vantrepotte, V., Chuprin, A., Grant, M., Jackson, T., & Sathyendranath, S. (2017). Assessing the fitness-for-purpose of satellite multi-mission ocean color climate data records: A protocol applied to OC-CCI chlorophyll-a data. *Remote Sensing of Environment*, *203*, 139–151.

Mélin, F., Vantrepotte, V., Clerici, M., D'Alimonte, D., Zibordi, G., Berthon, J. F., & Canuti, E. (2011). Multi-sensor satellite time series of optical properties and chlorophyll-a concentration in the Adriatic Sea. *Progress in Oceanography*, *91*(3), 229–244. https://doi.org/10.1016/j.pocean.2010.12.001

Mignot, A., Claustre, H., Uitz, J., Poteau, A., D'Ortenzio, F., & Xing, X. (2014). Understanding the seasonal dynamics of phytoplankton biomass and the deep chlorophyll maximum in oligotrophic environments. A Bio-Argo float investigation. *Global Biogeochemical Cycles*, *28*, 856–876. https://doi.org/10.1002/2013GB004781

Morel, A. (1988). Optical modeling of the upper ocean in relation to its biogenous matter content (case I waters). *Journal of Geophysical Research*, *93*(C9), 10749–10,768. https://doi.org/10.1029/JC093iC09p10749

Nelson, N. B., Siegel, D. A., & Michaels, A. F. (1998). Seasonal dynamics of colored dissolved material in the Sargasso Sea. *Deep Sea Research, Part I*, *45*(6), 931–957. https://doi.org/10.1016/S0967-0637(97)00106-4

Pitarch, J., Bellacicco, M., Volpe, G., Colella, S., & Santoleri, R. (2016). Use of the quasi-analytical algorithm to retrieve backscattering from in-situ data in the Mediterranean Sea. *Remote Sensing Letters*, *7*(6), 591–600. https://doi.org/10.1080/2150704X.2016.1171922

Roesler, C. S., Perry, M. J., & Carder, K. L. (1989). Modeling in situ phytoplankton absorption from total absorption spectra in productive inland marine waters. *Limnology and Oceanography*, *34*(8), 1510–1523. https://doi.org/10.4319/lo.1989.34.8.1510

Sathyendranath, S., Brewin, R. J., Jackson, T., Mélin, F., & Platt, T. (2017). Ocean-colour products for climate-change studies: What are their ideal characteristics? *Remote Sensing of Environment*, *203*, 125–138.

Siegel, D. A., Behrenfeld, M. J., Maritorena, S., McClain, C. R., Antoine, D., Bailey, S. W., et al. (2013). Regional to global assessments of phytoplankton dynamics from the SeaWiFS mission. *Remote Sensing of Environment*, *135*, 77–91. https://doi.org/10.1016/j.rse.2013.03.025

Siokou-Frangou, I., Christaki, U., Mazzocchi, M. G., Montresor, M., Ribera d'Alcalá, M., Vaqué, D., & Zingone, A. (2010). Plankton in the open Mediterranean Sea: A review. *Biogeosciences*, *7*(5), 1543–1586. https://doi.org/10.5194/bg-7-1543-2010

Sosik, H. M. (2008). Characterizing seawater constituents from optical properties. In M. Babin, C. S. Roesler, & J. J. Cullen (Eds.), *Real-time coastal observing systems for ecosystem dynamics and harmful algal blooms* (pp. 281–329). Paris, France: UNESCO. (peer reviewed)

Sosik, H. M., & Mitchell, B. G. (1995). Light absorption by phytoplankton, photosynthetic pigments, and detritus in the California Current System. *Deep Sea Research*, *42*(10), 1717–1748. https://doi.org/10.1016/0967-0637(95)00081-G

Stramski, D., Boss, E., Bogucki, D., & Voss, K. J. (2004). The role of seawater constituents in light backscattering in the ocean. *Progress in Oceanography*, *61*(1), 27–56. https://doi.org/10.1016/j.pocean.2004.07.001

Stramski, D., & Kiefer, D. A. (1991). Light scattering by microorganisms in the open ocean. *Progress in Oceanography*, *28*(4), 343–383. https://doi.org/10.1016/0079-6611(91)90032-H

Thomalla, S. J., Ogunkoya, G., Vichi, M., & Swart, S. (2017). Using optical sensors on gliders to estimate phytoplankton carbon concentrations and chlorophyll-to-carbon ratios in the Southern Ocean. *Frontiers in Marine Science*, *4*, 34. https://doi.org/10.3389/fmars.2017.00034

Volpe, G., Nardelli, B. B., Cipollini, P., Santoleri, R., & Robinson, I. S. (2012). Seasonal to interannual phytoplankton response to physical processes in the Mediterranean Sea from satellite observations. *Remote Sensing of Environment*, *117*, 223–235. https://doi.org/10.1016/j.rse.2011.09.020

Volpe, G., Santoleri, R., Vellucci, V., d'Alcalà, M. R., Marullo, S., & d'Ortenzio, F. (2007). The colour of the Mediterranean Sea: Global versus regional bio-optical algorithms evaluation and implication for satellite chlorophyll estimates. *Remote Sensing of Environment*, *107*(4), 625–638. https://doi.org/10.1016/j.rse.2006.10.017

Westberry, T., Behrenfeld, M. J., Siegel, D. A., & Boss, E. (2008). Carbon-based primary productivity modeling with vertically resolved photoacclimation. *Global Biogeochemical Cycles*, *22*, G82024. https://doi.org/10.1029/2007GB003078

Westberry, T. K., Dall'Olmo, G., Boss, E., Behrenfeld, M. J., & Moutin, T. (2016). Coherence of particulate beam attenuation and backscattering coefficients in diverse open ocean environments. *Optics Express*, *18*(15), 15,419–15,425.